Protein Engineering, Design and Selection, 2021, **34**, 1–11
https://doi.org/10.1093/protein/gzab030
Original Article

peds
protein engineering design & selection

Generation of a nanobody against HER2 tyrosine kinase using phage display library screening for HER2-positive breast cancer therapy development

Thomanai Lamtha[1], Lueacha Tabtimmai[2], Kunan Bangphoomi[1], Duangnapa Kiriwan[1], Aijaz A Malik[3], Wanpen Chaicumpa[4], Paul M.P. van Bergen en Henegouwen[5] and Kiattawee Choowongkomon[1,6,*]

[1]Department of Biochemistry, Faculty of Sciences, Kasetsart University, Laboratory of Protein Engineering and Bioinformatics, Chatuchak, Bangkok 10900, Thailand
[2]Department of Biotechnology, Faculty of Applied Science, King Mongkut's University of Technology North Bangkok, Bang Sue, Bangkok 10800, Thailand
[3]Center of Data Mining and Biomedical Informatics, Mahidol University, Salaya, Nakhon Pathom, 73170, Thailand
[4]Department of Parasitology, Faculty of Medicine Siriraj Hospital, Mahidol University, Laboratory for Research and Technology Development, Bangkok Noi, Bangkok 10700, Thailand
[5]Cell Biology, Neurobiology and Biophysics, Department of Biology, Faculty of Science, Utrecht University, Utrecht 3584 CH, the Netherlands
[6]Center for Advanced Studies in Nanotechnology for Chemical, Food and Agricultural Industries, KU Institute for Advanced Studies, Kasetsart University, Chatuchak, Bangkok 10900, Thailand
*To whom correspondence should be addressed. E-mail: kiattawee.c@ku.th

Abstract

Human epidermal growth factor receptor 2 (HER2) protein overexpression is found in ~30% of invasive breast carcinomas and in a high proportion of noninvasive ductal carcinomas *in situ*. Targeted cancer therapy is based on monoclonal antibodies and kinase inhibitors and reflects a new era of cancer therapy. However, delivery to tumor cells *in vivo* is hampered by the large size (150 kDa) of conventional antibodies. Furthermore, there are many disadvantages with the current anti-HER2 drug, including drug resistance and adverse effects. Nanobodies (15 kDa), single-domain antibody (sdAb) fragments, can overcome these limitations. This study produced the recombinant sdAb against the HER2-tyrosine kinase (HER2-TK) domain using phage display technology. Three specific anti-HER2-TK sdAbs were selected for further characterization. Hallmark V_HH residue identification and amino acid sequence analysis revealed that clone numbers 4 and 22 were VH antibodies, whereas clone number 17 was a V_H H antibody (nanobody). The half-maximal inhibitory concentration of V_HH17 exhibited significantly greater HER2 kinase-inhibition activity than the other clones. Consistent with these results, several charges and polar residues of the HER2-TK activation loop that were predicted based on mimotope analysis also appeared in the docking result and interacted via the CDR1, CDR2 and CDR3 loops of V_HH17. Furthermore, the cell-penetrable V_HH17 (R9 V_HH17) showed cell-penetrability and significantly decreased HER2-positive cancer cell viability. Thus, the V_H H17 could be developed as an effective therapeutic agent to treat HER2-positive breast cancer.

Keywords: cell-penetrating peptide, Human epidermal growth factor receptor 2 (HER2), mimotope mapping, molecular docking, nanobody, phage display library screening, tyrosine kinase

Introduction

Human epidermal growth factor receptor 2 (HER2; also known as Neu or ErbB2) is a member of the epidermal growth factor receptor (EGFR; also known as ErbB) family of receptor tyrosine kinases, which, in humans, includes HER1 (EGFR or ERBB1), HER2, HER3 (ERBB3) and HER4 (ERBB4) (Yu and Hung 2000). It plays a key role in the HER family, cooperating with other HER receptors via a complex signaling network to regulate cell growth, differentiation and survival, and its inappropriate activation is associated with the development and severity of many cancers (Yarden and Sliwkowski 2001; Roskoski 2004; Bose 2013; Ross *et al.*, 2013). HER2 overexpression is found in ~20%–30% of human breast cancers and is correlated with more aggressive tumors and a poorer prognosis (Ross *et al.*, 2009; Slamon *et al.*, 1987; Turke *et al.*, 2012; Yu and Hung 2000). The treatment of breast cancer relies on a multimodality approach, including surgery, radiation, hormone therapy, chemotherapy and supportive therapy (Arteaga *et al.*, 2012).

HER2 is an interesting target for cancer treatment. The anti-HER2 monoclonal antibody, known as either Trastuzumab (Herceptin®) or Pertuzumab (Perjeta®), has been developed for treating HER2-positive early-stage and metastatic breast cancers (Bachelot *et al.*, 2019; Capelan *et al.*, 2013; Ferretti *et al.*, 2006; Joensuu *et al.*, 2006; Von Minckwitz *et al.*, 2017). However, several practical drawbacks for its clinical use are apparent, including its large size (~150 kDa), which results (i) in weak binding when small-size protein antigens are not easily recognized by the concave surfaces of complementarity-determining region (CDR) loops and (ii) in difficult penetration of dense tissues such as solid tumors (Sarma *et al.*, 1971). Additionally, the extracellular domain-targeted drug cannot overcome breast cancer metastasis because the monoclonal antibody is unable to penetrate the blood–brain barrier, which is a target organ for metastasis cancer cells. Furthermore, expensive production costs have hampered the extensive use of antibodies in such platforms (Baker *et al.*, 2008; Rudnick and Adams 2009). Small-molecule tyrosine kinase

Received: March 16, 2021. **Revised:** November 8, 2021. **Editorial decision:** November 8, 2021

inhibitors (TKIs) such as Sorafenib (Nexavar®) and Lapatinip (Tykerb®) target the TK domain of the EGFR family (Hudelist *et al.,* 2003; Yarden and Sliwkowski 2001). Drugs targeting the TK domain can solve trastuzumab resistance resulting from truncated HER2 and dimerization of the EGFR family (Blackwell *et al.,* 2010; O'Donovan *et al.,* 2011). However, there are many drawbacks associated with the current anti-HER2 drugs, including the mutation of the HER2-TK domain (T7981, L755S) associated with lapatinib resistance (Bose *et al.,* 2013; D'Amato *et al.,* 2015), cardiac toxicity (Smith *et al.,* 2006; Speyer 2002) and a number of adverse effects (Dawood *et al.,* 2007; Marty *et al.,* 2005). These current limitations make it important to discover new drugs and biomolecules for cancer treatment.

Recently, single-domain antibodies derived from the variable domains of Camelidae heavy-chain-only antibodies (V_H H) have been extensively researched for diagnostic and therapeutic purposes. Nanobodies are small (15 kDa), single-domain fragments possessing the full antigen binding capacity of monoclonal antibodies when expressed recombinantly. Based on these features, nanobodies are becoming a more promising tool for the diagnosis and therapy of various diseases compared with conventional antibodies (Revets *et al.,* 2005; Siontorou 2013). Nanobodies can be easily cloned and selected from immune or naïve V_HH libraries because of their single-domain nature and strict monomeric behavior. Generally, further isolation of nanobody clones with high specificity is performed through phage display technology (Hoogenboom *et al.,* 1998; Reiter *et al.,* 1999). In 2010, the first isolation of a nanobody with high affinity to the HER2-extracellular domain(HER2-ECD) was reported; this nanobody reacted with native antigen presented on the surface of the HER2-positive SKBR-3 cell line (Sheikholeslami *et al.,* 2010). Since then, many more studies have been applied to HER2-ECD in the diagnosis and treatment of cancer (Vaneycken *et al.,* 2011; Pruszynski *et al.,* 2014, 2018; Xavier *et al.,* 2016; D'Huyvetter *et al.,* 2017; Altunay *et al.,* 2020). In this article, the nanobodies that bind the HER2-TK domain were identified for the first time. Subsequently, the DNA of the screened nanobodies was subjected to DNA sequencing and used for computational analysis. The selected clones (VH4, VH22 and V_HH17) of the anti-HER2-TK domain VH/V_HH were subjected to a kinase-inhibition assay. Despite only one-round of bio-panning, the identified nanobody exhibits the binding specificity, affinity and kinase-inhibition activity against recombinant HER2-TK. Additionally, the nanobody were humanized and tagged with cell-penetrable peptide(R9) to minimize the effects of immune response and promotes the nanobody to enter cancer cells. We further demonstrated the cell-penetrability and growth-inhibition activity of R9-V_HH17 on HER2-positive cancer cells. Finally, molecular docking and mimotope analysis were used to study the interaction between HER2-TK and V_HH17. Overall, this study suggests that the V_HH17 nanobody is efficient and can be developed as an HER2-TK-targeted inhibitor.

Materials and Methods

Selection of the nanobody against HER2-TK using the bio-panning technique

The purified recombinant protein of human HER2/ErbB2 (Lys676-Val1255) kinase was purchased from Sino Biological Inc. (Beijing, China). The HER2-TK recombinant protein was used as the targeted antigen to select the antibody from the humanized VH/V_HH phage display library obtained from Prof. Dr Wanpen Chaikumpa (Department of Parasitology, Faculty of Medicine Siriraj Hospital, Mahidol University, Bangkok, Thailand). The preparation of phage display library was proceeded following previous report. Briefly, the peripheral blood mononuclear cells were isolated from 50 ml of venous blood collected from an 8-month-old naïve male dromedary (*Camelus dromedarius*). The total RNA was extracted from the cells by TRIzol™ reagent (Invitrogen), and the mRNA was reverse transcribed to cDNA using Revert Aid™ (Fermentas Life Sciences). The gene fragments encoding variable domains of the dromedary VH/V_HH were polymerase chain reaction (PCR) amplified using the cDNA as template, as well as 14 forward and three reverse human immunoglobulin-specific primers (Kulkeaw *et al.,* 2009). A heavy-chain antibody fragment (VH/VHH) phage display library was constructed by amplification of the immunoglobulin genes of a nonimmune camel, *C. dromedarius*, using primers specific to human VH gene segments (Thanongsaksrikul *et al.,* 2010) Single round of selection was performed, 1 µg of recombinant HER2 protein was immobilized on a microtiter plate with coating buffer. After 16–18 h, the excess protein was removed by extensively washing. Adding blocking buffer was performed for 30 min. At the indicated time, the well was twice washed with PBS containing 0.05% Tween 20 (PBS-T). The library was prepared by 10-fold dilution with PBS-T to reach $\sim 1 \times 10^{11}$ colony forming units. One hundred microlitres of the diluted phage library was added in the HER2-TK-immobilized well and continually incubated at 37°C for 1 h. After phage enrichment, unbound phages were discarded by extensively washing with PBS containing 0.1% Tween 20 (PBS-T). After 10-time washing, bound phages were eluted by adding log-phase *E. coli* HB2151. The infected *E. coli* HB2151 were spread on Luria–Bertani (LB) agar containing 100 µg/ml Ampicillin. After 16–18 h, growing colonies were picked as positive clones for further investigation.

Screening of the VH/V_HH-expressing HB2151 *E. coli* clone

The VH/V_HH-expressing HB2151 *E. coli* clone was determined using a PCR technique. The bacterial colonies were used as a template for PCR analysis. For VH/V_HH amplification, the following oligonucleotide primers were used: pCANTAB5-R1 (5′-CCA TGA TTA CGC CAA GCT TTG GAG CC-3′), which bound specifically to the pCANTAB5E vector near the 5′ end of the *Sfi I* restriction endonuclease site, and the reverse nucleotide primer pCANTAB5-R2 (5′-GCT AGA TTT CAA AAC AGC AGA AAG G-3′), which bound specifically to the pCANTAB5E vector near the 3′ end of the *Not I* restriction endonuclease site. The PCR product was analyzed using agarose gel electrophoresis. The expected length of VH/V_HH was 600 base pairs.

Plasmid extraction and DNA sequencing

The VH/V_HH-expressing bacterial colony that provided the TK-inhibiting activity was subjected to plasmid extraction using the alkaline lysis method. The plasmid DNA concentration was determined by measuring the optical density (OD) at A260 nm and subjecting the sample to DNA sequencing.

Expression of VH/VHH

The *E. coli* strain HB2151 that provided VH/V_HH was picked and inoculated into 10 ml of LB-AG broth at 37°C for 8 h. A sample (500 µl) of incubated culture was inoculated into fresh LB-A broth and incubated at 37°C and 250 rpm in a shaking incubator until the OD at 600 nm equaled 0.5. Isopropyl-1-thio-β-D-galactopyranoside was added into the broth at a final concentration of 1 mM. The broth was incubated at 37°C and 250 rpm in a shaking incubator for 5 h. *E. coli* cells were collected using centrifugation at 4000 × *g* for 10 min at 4°C. The whole-cell lysate was prepared using sonication. The bacterial cell pellet was sonicated using an ultrasonic homogenizer LABSONIC P (Satorius AG, Germany). After sonication, the whole-cell lysate was centrifuged at 12 000 × *g* for 10 min at 4°C. The supernatant was collected as the soluble part. The pellet was collected as the insoluble part and was solubilized by boiling with 10% SDS. Both the soluble and insoluble parts were subjected to SDS-PAGE, western blot analysis, and affinity column purification.

Expression and purification of EGFR and HER2-TK

The pCold I vectors encoding EGFR-TK and HER2-TK were transformed into the *E. coli* strain Rosetta™ (DE3) Competent Cells (Seetaha *et al.*, 2019). The positive clone was picked and inoculated into 10 ml of LB-AG broth and incubated at 37°C overnight with gentle shaking. A sample (500 µl) of incubated culture was inoculated into fresh LB-A broth and incubated at 37°C and 250 rpm in a shaking incubator until the OD at 600 nm equaled 0.5. Isopropyl-1-thio-β-D-galactopyranoside was added into the broth to a final concentration of 0.5 mM. The broth was further incubated at 16°C and 250 rpm in a shaking incubator for 16–18 h. Cells were harvested using centrifugation and lysed using lysis buffer (50 mM Tris–HCl, pH 8.0, 1 mM β-mercaptoethanol, 50 mM NaCl, 5 mM $MgCl_2$, 1mMPMSF, 1mMEDTA, 0.5%Triton-X 100 and 5% glycerol) and sonication at 30% amplitude and 5 s pulse cycle for 30 min (Vibra-Cell™ Ultrasonic Liquid Processors) on ice. The supernatant was collected, filtered through a0.45-µm membrane, and purified using a DEAE-Sepharose column (Cytiva™), equilibrated with buffer A (50 mM Tris–HCl, pH 8.0, 1 mM β-mercaptoethanol, 50 mM NaCl, 5 mM $MgCl_2$, 1 mM EDTA and 5% glycerol), and eluted using a stepwise gradient from 0%–100% elution buffer (50 mM Tris–HCl, pH 8.0, 1 mM β-mercaptoethanol, 1 M NaCl, 5 mM $MgCl_2$, 1 mM EDTA and 5% glycerol). The most approximate molecular weight fraction was dialyzed against dialysis buffer (50 mM Tris–HCl, pH 7.4, 1 mM mercaptoethanol, 20 mM NaCl, 5 mM MgCl2, 1 mM EDTA and 5% glycerol) at 4°C overnight. Then, the dialysate was applied to a Resource™ Q column (16 mm diameter × 30 mm bed height), connected to an FPLC System (GE ÄKTA FPLC™), equilibrated with dialysis buffer (pH 7.4), and eluted using a linear gradient of 0%–30% elution buffer. The fractions were tested for activity, and those of interest were collected. Gel filtration chromatography (Superdex™ 200 pg) was used to separate soluble proteins as a final purification step. The eluted peaks were further tested for kinase activity (ADP-Glo™).

Indirect ELISA

For candidate nanobody selection, 2 µg of HER2-TK, EGFR-TK and Janus kinase 2 (JAK2, Merck Millipore, MA, USA) recombinant protein was coated on an ELISA plate (E.I.A/R.I.A. 8-Well strip Flat bottom Corning, NY, USA) as previously described in the bio-panning step. To eliminate any nonspecific binding signals, 1 µg of skim milk was coated on an ELISA plate as previously described in the bio-panning step. After the coating step, the unbound protein was discarded, and 300 µl of blocking buffer (3% skim milk in PBS, pH 7.4) was added into the well and incubated at 25°C for 30 min. After removing the blocking buffer, the well was washed three times with washing buffer (PBS-T, pH 7.4). Next, 100 µl of cell lysate from VH/V_HH-expressing HB2151 *E. coli* were used as the test group, R2 (irrelevant nanobody) and HB2151 *E. coli* lysate were used as the control group. The sdAbs solution containing 50 µl of whole-cell lysate and 50 µl of PBS-T was added and incubated at 25°C for 1 h. After incubation, the well was washed three times with PBS-T. The HER2-TK, EGFR-TK and JAK2-bound sdAbs were detected using horseradish peroxidase-conjugated anti-E tag diluted in PBS-T at a dilution of 1:5000. After the incubation step at 25°C for 1 h, the well was washed three times with PBS-T. After the washing step, 50 µl of 2,2′-Azino-bis-(3-ethylbenzothiazoline-6-sulfonic acid) solution (Zymed Laboratories Inc., South San Francisco, CA, USA) was added into the well and incubated at 25°C for 30 min with light protection. The ELISA signal was measured at an OD of 450 nm using an ELISA reader (Multiskan EX, Labsystem, Midland, Ontario, Canada). For binding affinity determination, MaxiSorp Nunc-immuno 96-well ELISA plates were coated (100 µg/well) at 4°C overnight with purified recombinant HER2-TK. V_HH17 and a mixture of V_HH17 and lapatinib were then incubated starting at 1000 nM with 2-fold dilution for 1 h at 4°C. Rabbit anti-V_HH antibody (Creative Biolabs, Inc., New York, USA) was then added at a dilution of 1:1000 for 1 h at 25°C, followed by goat antirabbit IgG H&L (IRDye® 800CW; Abcam Plc., Cambridge, UK) at a dilution of 1:1000 for 1 h at 25°C in the dark. The fluorescence at 800 nm was measured using an Odyssey CLx Infrared Imaging System (LI-COR Biosciences). The median fluorescence intensities at each dilution were plotted, and data were analyzed using GraphPad Prism (GraphPad Software Inc., San Diego, CA, USA).

TK inhibition assay

The sdAbs were tested for their inhibitory activity against HER2-TK, EGFR-TK and JAK2 activity using the ADP-Glo™ Kinase Assay (Promega). The experimental process was performed according to the method described by the manufacturer. The reaction mixture (25 µl) contained 5 µl of kinase buffer (20 mM Tris–HCl (pH 7.5), 20 mM $MgCl_2$, 0.1 mg/ml BSA), 5 µl of 25 µM ATP, 5 µl of 12.5 µg/ml poly(Glu:Tyr) substrate, 5 µl of 1 ng/µl HER2-TK, EGFR-TK or JAK2 (diluted in kinase buffer), and 5 µl of various sdAbs concentrations. A well without HER2-TK was used as the negative control, and a well without inhibitors was used as the positive control kinase activity. Lapatinib, HER2-TKI or gefitinib EGFR-TKI (NCI, USA), were used as control kinase-inhibitor, R2 was used as the noninhibition nanobody. The reactions were performed in a 384-well plate (Greiner Bio-One Lumitrac plate, solid white) and incubated at room temperature for 1 h. Afterward, 5 µl of ADP-Glo reagent was added to terminate the kinase reaction and deplete the remaining ATP at room temperature for 40 min. Next, 10 µl of ADP-Glo detection reagent was added for 30 min to simultaneously convert

ADP to ATP and to allow the newly synthesized ATP to be measured using a luciferase/luciferin reaction. Luminescence measurements were made using a microplate spectrophotometer (Synergy HTX Multi-Mode reader, BioTek, VT, USA). The half-maximal inhibitory concentration (IC_{50}) values of inhibitors were determined using the nonlinear regression curve fit in GraphPad Prism (GraphPad Software Inc., San Diego, CA, USA).

Mimotope mapping of HER2-TK-specific nanobody

The wells of a 96-well plate (Nunc MaxiSorp) were coated with 100 µg/ml of purified nanobody in 0.1 M $NaHCO_3$ (pH 8.6) and incubated overnight at 4°C. Wells coated with buffer were used as negative controls. After the wells were washed with TBST (50 mM Tris–HCl (pH 7.5), 150 mM NaCl containing 0.1% Tween-20) and blocked with blocking buffer (0.1 M $NaHCO_3$ (pH 8.6), 5 mg/ml BSA) for 1 h at 4°C, 100 µl of Ph.D.-C7C™ Peptide libraries (New England Biolabs, MA, USA,) diluted (1:100) in TBST was added, and the plate was left at room temperature for 1 h. After removing unbound phage, the wells were washed, and the bound phages were eluted with elution buffer (0.2 M glycine-HCl (pH 2.2), 1 mg/ml BSA) for 10 min at room temperature and then neutralized with 30 µl of 1 M Tris–HCl (pH 8.5). The eluted phages were then amplified by adding 150 µl of mid-log-phase ER2738 *E. coli*, maintained at 25°C for 20 min, and the phage-infected *E.coli* were grown in LB broth at 37°C for 4.5 h. The PEG/NaCl precipitation method was used to collect propagated phages for the next panning rounds. The panning was repeated twice. The *E. coli* culture supernatants from the third round of bio-panning were plated on agarose topped-LB plates containing X-gal and isopropyl-1-thio-β-D-galactopyranoside. The phage clones were randomly picked for blue plaque and sequenced using the 96 gpIII Sequencing Primer. Consensus mimotope sequences were obtained by multiple alignments.

Molecular docking to determine the interactions between VHH17 and HER2-TK

Computerized intermolecular docking was used to determine the interactions between V_HH17 and HER2-TK. The crystal structure of HER2-TK was retrieved from RCSB, PDBID 3PP0, whereas the HER2-TK-bound V_HH17 was modeled using the RaptorX server (Källberg *et al.*, 2014). The modeled structure of the nanobody was further refined using the high-resolution protein structure refinement server, Modrefiner (Xu and Zhang 2011). Protein–protein docking between the 3D structure of HER2-TK and modeled V_HH17 was performed using clusopro 2.0 (Brenke *et al.*, 2012). Molecular docking was predicted in four separate modes (balance, electrostatic-favored, hydrophobic-favored and Van der Waals), and the ones with the lowest energy scores were selected. Docking models were analyzed using the PyMOL program (PyMOL System, Version 1.3r1 edu, Schrodinger, LLC, NY, USA). Interaction profiles of the docked results were analyzed using LigPlot+ (Laskowski and Swindells 2011).

Cell-penetrating peptide tagging and cell viability assay

We next assessed whether our nanobody could inhibit cancer cell proliferation and induce cancer cell death. The anti-HER-TK V_HH17 genes of HB2151 *E. coli* clones that bound and blocked the activity of TKs were linked to the arginine-rich, cell-penetrating peptide nona-arginine (R9). The VH/V_HH sequences isolated from the pCANTAB-5E phagemids of the HB2151 *E. coli* clones were ligated into pLATE52 plasmids downstream of the R9-coding sequence using the ligation-independent cloning method. This resulted in His6-T7-R9-V_HH17, with R9 providing cell-penetrating peptides, allowing internalization of the nanobody to target cells, and the His6-T7 tag allowing Ni-based purification and T7 Epitope Tag-based detection. His6-T7-R9-V_HH17 expression was induced via standard methods in the *E. coli* strain Rosetta™ (DE3) Competent Cells. Cells were harvested using centrifugation at 4000 rpm and 4°C for 30 min, resuspended in ice-cold lysis buffer, and incubated for 15 min on ice. Then, the bacteria were lysed using sonication at 30% amplitude and a 5 s pulse cycle for 20 min (Vibra-Cell™ Ultrasonic Liquid Processors) on ice. The supernatant was collected, and protein was purified using Ni-NTA Agarose beads.

Cell growth was assayed using the alamarBlue™ cell viability assay in four cancer cell lines with different HER2 expression levels: the murine fibroblast cell line NIH/3 T3, the triple-negative breast cancer cell line MDA-MB-231, the epidermoid carcinoma cell line A431 (EGFR-positive), and the human breast carcinoma cell line BT-474 (HER2-positive). Cells were plated in 96-well microtiter plates (100 µl/well) at initial densities of 5×10^4 cells/ml. After 24 h in culture, the monolayer of cells in the plate was exposed to 100 µl of DMEM containing different concentrations of Lapatinib, R2 (irrelevant nanobody), V_HH17 and R9-V_HH17 (2-fold dilutions, starting at 1 µM). After another 72 h in culture, alamarBlue™ Cell Viability Reagent was added directly into the culture medium at a final concentration of 10%, into the medium without cells (negative control), or to untreated cells (positive control). The plate was returned to the incubator for 4 h. The intensity of fluorescence produced by cell dehydrogenases is directly proportional to the number of living cells respiring. Absorption of the samples was measured using a spectrophotometer (BioTek Synergy HTX) with excitation and emission wavelengths of 550 and 590 nm, respectively.

Estimation of nanobody binding affinity

The binding affinity between nanobodies and HER2-TK or EGFR-TK(nonrelated kinase) were estimated using an Open SPR 2-Channel Starter Pack R4.2(Nicoya). Different concentrations of nanobody were injected into the flow-channel and then passed over the HER2-TK-immobilized Sensor Amine Chip (NECTEC, NSTDA). Briefly, EDC/NSH coupling HER2-TK or EGFR-TK (100 µg/ml) was immobilized on an Amine Sensor Chips (Nicoya) at 4000 response units (RU) at a flow rate of 20 µl/min in PBS-buffer (pH 7.4), sterile filtered and degassed (running buffer). For determination of binding kinetics, the recombinant nanobody at various concentrations were flown at 30 µl/min over the chip surface in the PBS-buffer (pH 7.4). For the lapatinib, the PBS-buffer with 5% DMSO were used as dilution and running buffer. The sensorgrams with different concentrations of analyte were analyzed using the Trace Drawer 1.9.1 software (Ridgeview Instruments).

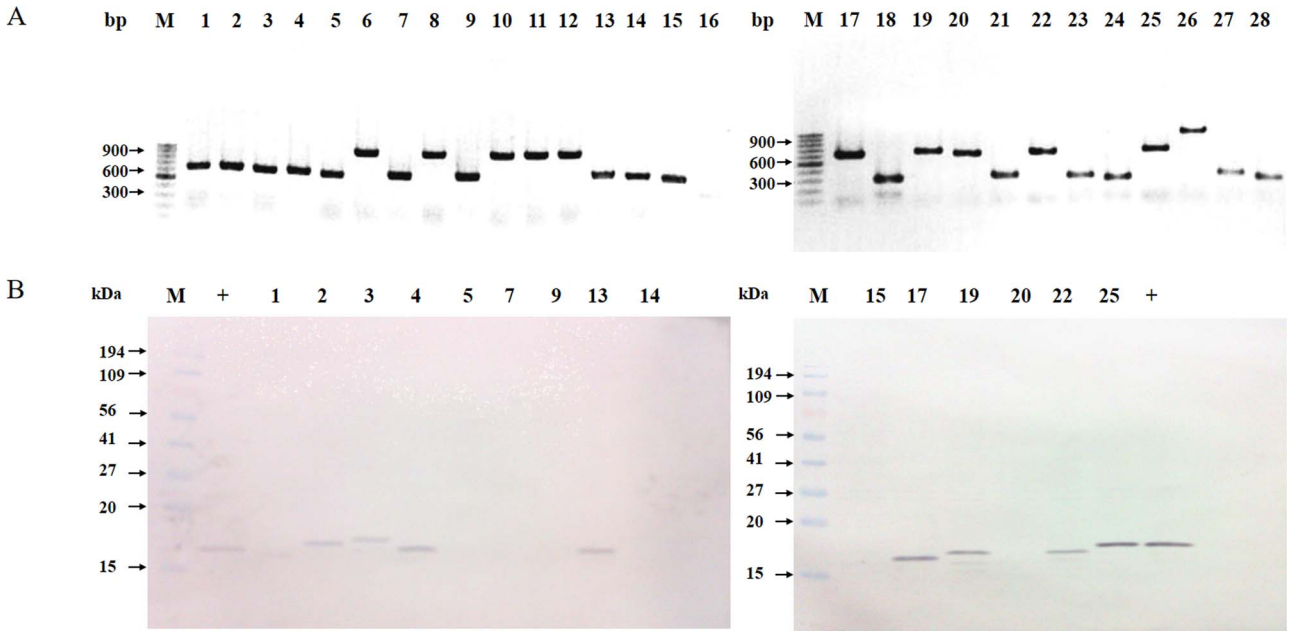

Fig. 1. VH/VHH clones screened using bio-panning. (A) Agarose gel electrophoresis of PCR product shown in inverted color. Lane M: 100 bp DNA ladder; lanes 1–28: PCR products of positive colonies containing the target gene (expected size of VH/VHH gene is 600 bp). (B) Western blot analysis of the VH/VHH-expressing HB2151 *E. coli* clone. Lane M: prestained protein molecular weight marker. Lane +: VH/VHH antibody.

Results

The HB2151 *E. coli* clone carrying the VH/V_HH gene

From the LB-AG agar plates, the bio-panning experiment produced 28 HB2151 *E. coli* colonies, which were subjected to analysis of the VH/V_HH gene using a PCR technique with the pCANTAB5-R1 and R2 primers. Figure 1A shows the PCR products of the VH/V_HH gene. Based on the agarose gel electrophoresis, bacterial colony clone numbers 1, 2, 3, 4, 5, 7, 9, 13, 14, 15, 17, 19, 20, 22 and 25 provided a positive DNA band at 600 bp, indicating that they carried the VH/V_HH genes. The percentage of positive colonies from the LB-AG agar plate was 53.57%. These colonies were subjected to the expression of the VH/V_HH antibody.

The VH/V_HH-expressing HB2151 *E. coli* clone

The 15 bacterial colonies carrying the VH/V_HH genes were subjected to VH/V_HH protein expression. The proteins from the VH/V_HH-expressing HB2151 *E. coli* clones were separated with 12% polyacrylamide gel under reducing conditions. The antibodies were transferred onto NC membranes and incubated with mouse anti-E tag monoclonal antibodies. Figure 1B shows the western blot analysis of the HB2151 *E. coli* colonies carrying the VH/V_HH genes. The expected size of the VH/V_HH antibody was 15–20 kDa, and nine colonies (clone numbers 1, 2, 3, 4, 13, 17, 19, 22 and 25) had protein bands of 15–20 kDa, indicative of the VH/V_HH antibody. The VH/V_HH antibodies were used to determine the binding activity with ELISA. The percentage of positive colonies that provided VH/V_HH antibodies was 64.2%. The variation in the size of the protein band was due to different numbers of amino acid residues in the CDR.

The determination of VH/V_HH specificity against HER2-TK

Both the binding and inhibitory properties of the nanobody were investigated. VH/V_HH antibody samples from HB2151 *E. coli* colony numbers 1, 2, 3, 4, 13, 17, 19, 22 and 25 were investigated for their binding affinity using the indirect ELISA technique. The cell lysate of HB2151 *E. coli* and R2 was used as a negative control. Figure 2 shows the ODs of the VH/V_HH antibody against BSA, HER2-TK, EGFR-TK and JAK2. Among these sdAbs, the clone numbers 17 exhibiting the highest specificity to HER2-TK, and higher than EGFR-TK and JAK2(irrelevant kinase), followed by the clone numbers 4 and 22. However, numbers 4 and 22 show similar binding affinity to HER2-TK and EGFR-TK. Thus, they were selected as candidates to further determine the IC_{50} using kinase activity inhibition assay.

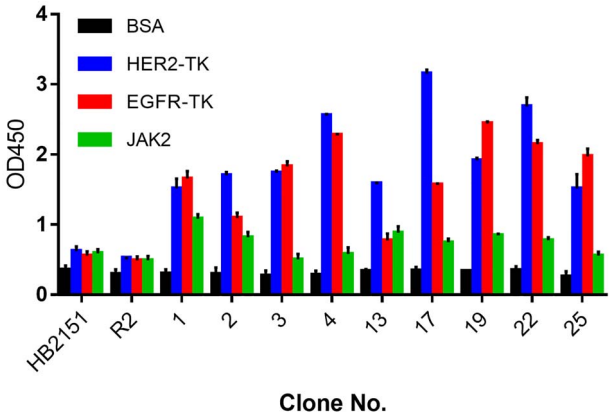

Fig. 2. Optical density at 450 nm (OD450) of indirect ELISA binding determination of HER2-TK, EGFR-TK and JAK2 interactions with the screened sdAbs. The binding signal of sdAbs and bovine serum albumin (BSA) and JAK2 (irrelevant kinase), were used to determine the nonspecific binding of sdAbs, R2 (irrelevant nanobody) and HB2151 *E. coli* lysate were used be negative control. Error bars indicate ± standard deviation of triplicate experiments.

```
                FR1                    CDR1        FR2          CDR2
VH4     QVQLVESGGGLVQPGGSLRLSCAASGFTFSNYHMSWVRQAPGKRLEWVSMINSAG--TYYTDSV
VHH17   QVQLVESGGGSVQAGGSLRLSCAASGYTYSSSCMGWFRQAPGKEREGVAGIKSTGGSKNYADSV
VH22    EVQLVESGAEVRKPGESLRISCKASGYTFSSYWIAWVRQMPGKGLEWMGIIYPGDFDTKYSPSF
        :*******.   :.* ***:** ***:*:*.  :.*.** ***  * :. * . .  . *: *.
                FR3                                CDR3          FR4
VH4     RGRFTISRDNAMNTLYLQMNNLKDEDTAVYSCATTWWWLP----------TDYWGQGTMVTVSS
VHH17   KGRFTISQDNAKNTVYLQMNSLKPEDTAIYYCAAKYGGICSWGAILGVREYNYWGQGTLVTVSS
VH22    RGQVTISADRSISTAYLQWSSLKASDTAIYYCARSPSGTTYWY------HFDDWGRGTTVTVSS
        :*:.*** *.: .* *** ..** .***:* ** .                : **:** *****
```

Fig. 3. Amino acid sequence alignment of antibody clone numbers 4, 17 and 22. The framework regions are black. CDR1, CDR2 and CDR3 are red, orange and purple, respectively. The fourth VHH tetrad residues located in framework 2 and additional VHH hallmark residues located in framework 1 are highlighted in yellow. Cysteine is shown in blue letters.

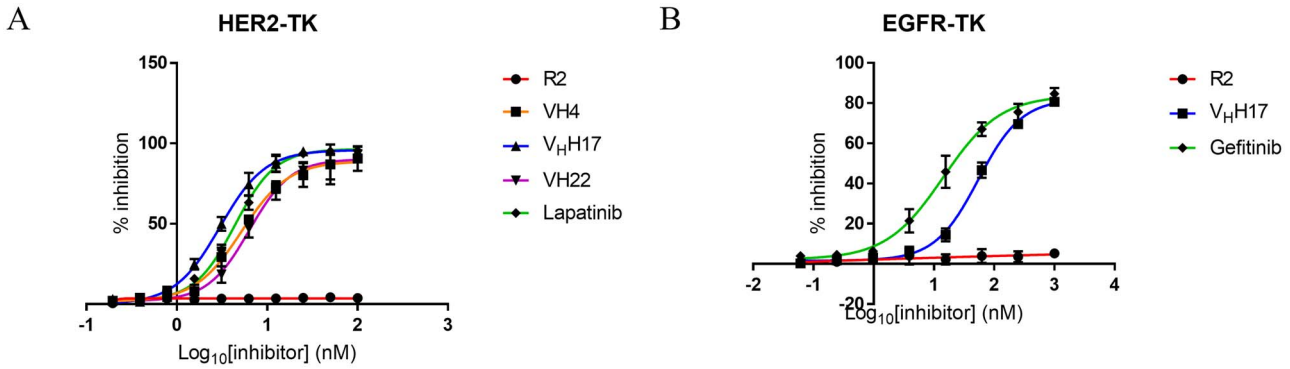

Fig. 4. Half-maximal inhibitory concentrations (IC50) for sdAbs, and TKIs. Graphs were plotted as percentage inhibition of kinase activity versus log of dose. (A). The IC50 values against HER2-TK are 5 nM (VH4), 3 nM (VHH17), 6 nM (VH22) and 4 nM (lapatinib). (B). The IC50 values against EGFR-TK are 55 nM (VHH17) and 14 nM (gefitinib), R2, the irrelevant nanobody showed no inhibition activity. The results are expressed as mean ± SD of triplicate experiments and estimated using GraphPad Prism (GraphPad Software Inc., San Diego, CA, USA).

Sequences analysis of VH/V_HH

Three VH/V_HH antibody clones (numbers 4, 17 and 22) showed binding against HER2-TK and were subjected to DNA sequencing. Next, the amino acid sequence alignments of these antibodies were deduced (Fig. 3). Various types of camelid antibodies (conventional and heavy-chain) exist, and the VH/V_HH antibody could be classified using the characterization of the VH and V_HH antibodies. V_HH from a heavy-chain antibody provided mutations of hydrophobic amino acids at residue numbers 42, 49, 50 and 52. These residues were located at framework 2. These mutations comprised V42F/Y, G49E, L50R/C and W52G/L (Fig. 3, highlighted in yellow). The amino acid sequence analysis revealed that clone numbers 4 and 22 were VH antibodies (VH4 and VH22, respectively), whereas clone number 17 was a V_HH antibody (V_HH17).

Inhibition activity of nanobody against HER2-TK

Although the binding properties of VH/VHH antibodies to the HER2-TK domain were indirectly determined using ELISA, the study of nanobody properties for inhibiting enzyme activity should be further investigated to screen for nanobodies with both binding and inhibitory properties. Thus, the TK activity inhibiting assay is an appropriate technique to investigate the inhibitory property of the antibody. The VH4, VH22 and V_HH17 proteins that were purified from the *E. coli* strain Rosetta™ (DE3) for colony numbers 4, 17 and 22 were subjected to TK activity inhibiting assay. VH4, VH22 and V_HH17 could inhibit the TK activity of HER2-TK with IC_{50} values of 5, 3 and 6 nM, respectively. Additionally, V_HH17 had the highest inhibitory activity, followed by VH4 and VH22 (Fig. 4A). The V_HH17 was further conducted to estimation of specificity against EGFR-TK and JAK2 (irrelevant kinase), the results showed that V_HH17 inhibits EGFR-TK and JAK2 with lower inhibition activity than HER2-TK, IC_{50} values of 55 and 554 nM, respectively. (Fig. 4B, Supplement Fig. 2). Thus, V_HH17 was selected as the best candidate for further testing. An ELISA assay was conducted to evaluate the binding affinity of V_HH17 alone and the same amounts of lapatinib mixed with V_HH17 against HER2-TK. V_HH17 alone showed ~6-fold higher binding affinity than that of V_HH17 combined with lapatinib (Fig. 5). This indicates that there is a possible binding site overlap between V_HH17 and lapatinib.

The interaction between V_HH17 and HER2-TK

To understand the mechanistic interpretation of specific nanobody, it is important to understand the atomistic interaction between the target protein (HER2-TK) and the specific nanobody (V_HH17). One possible way of doing this is using phage-mimotope searching to identify the potential binding site for V_HH17 by determining a phage peptide that can specifically bind to V_HH17. Seven phage clones with

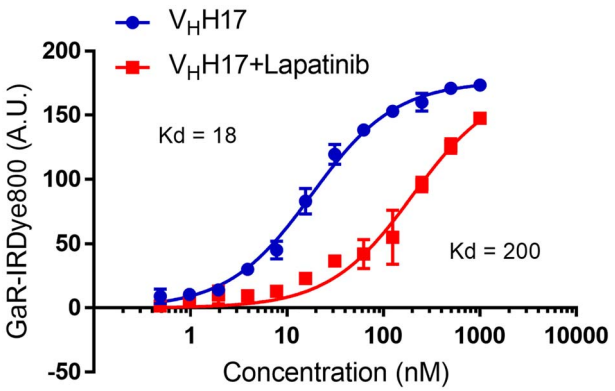

Fig. 5. Binding affinity of VHH17 alone and VHH17 mixed with lapatinib against HER-TK, tested with ELISA. The results are expressed as mean ± SD of triplicate experiments.

Table I. Mimotope peptides selected from the Ph.D.-C7C™ Peptide libraries using V_HH17

Number	Mimotope sequence	Occurrence
P1	SSAPSSRHEVSL	1
P2	QVPSSFYRAPNY	2
P3	FAPKMDYISSSQ	1
P4	AFAFGPMGSSAA	1
P5	LPYKIPSTFFNI	1
P6	SYGTTSGSLKFA	1
P7	AITDFSRSRDAG	1

12 residue peptides capable of binding with VHH17 were chosen and labeled as mimotopes: P1 (SSAPSSRHEVSL), P2 (QVPSSFYRAPNY), P3 (FAPKMDYISSSQ), P4 (AFAFGPMGSSAA), P5 (LPYKIPSTFFNI), P6 (SYGTTSGSLKFA) and P7 (AITDFSRSRDAG) (Table I) were submitted to the Pepitope webserver using the pepsurf and mapitope algorithm to predict the binding site. The results cluster was shown in Supplement Fig. 6. According to its score, cluster number 1 contains crucial residues of structural motifs and loops that play critical roles in its activation and generate conformational changes within the cytoplasmic domain of HER2-TK (Stamos *et al.*, 2002), which consists of five residues: Ala730, Phe731, Pro761, Lys762 and Ala763. The docking site has been used with these residues.

To gain greater insight into the molecular interactions between HER2-TK and V_HH17, computerized intermolecular docking was conducted to identify the presumptive residues of HER2-TK and the neutralizing sdAbs. The docking results indicated that V_HH17 interacted with the Phosphate-binding loop (Ser728, Ala730 and Ala734), the alpha C helix (Arg756, Glu757, Asn758, Ser760, Ala763, Glu766 an Ile767), catalytic loop (Arg844 and Arg849) of HER2-TK as shown in Fig. 6. Table II shows the predictive residue interactions between V_HH17 with HER2-TK along with the mode of interaction. The computational analysis clearly showed that V_HH17 interacted more specifically with the activation loop of HER2-TK.

Furthermore, V_HH17 was bound specifically with the activation loop of HER2-TK through its CDR1, CDR2 and CDR3 loops, whereas several polar residues formed hydrogen Hydrophobic interaction and Cation–π interaction. Mostly charged residues on the activation loop (Fig. 6 and Table II).

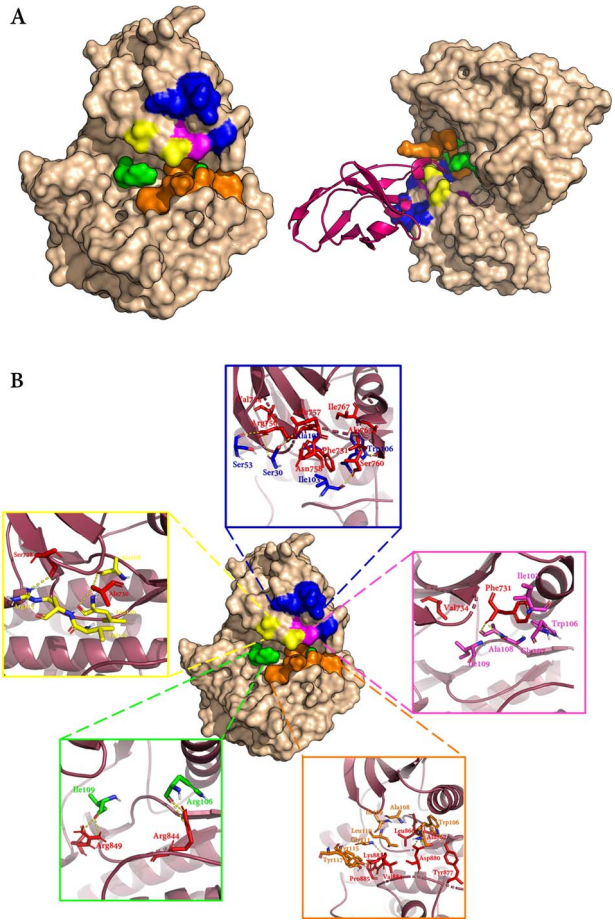

Fig. 6. Interaction plot of HER2-TK and VHH17 using molecular docking. (A) Surface representation of HER2-TK bound to VHH17. Multicolored contact region refers to the residue mapped by the binding loops of VHH17. (B) Structural visualization of the intermolecular contacts of the HER2-TK A-loop and nearby residues to VHH17. Dashed yellow lines indicate potential hydrogen bonds and hydrophobic and Cation–π interaction between the HER2-TK activation loop (red residues) and antigen binding of VHH17 (interacted with Phosphate-binding loop in yellow and purple, interacted with—Helix C in blue, interacted with catalytic loop and activation loop in green and blue residues, respectively). The model was analyzed with PyMOL1.3rl edu (The PyMOL Molecular Graphics System, Schrodinger, LLC, NY, USA).

Most importantly, the charged and polar residues of the activation loop (Gly865, Leu866 Ala867, Tyr877, Asp880, Lys883, Val884 and Pro885) could interact with the corresponding residues of the nanobody.

Cell-penetrable nanobodies reduced HER2-positive cell viability

Because V_HH17 was selected against the recombinant purified HER2-TK domain, its function regarding HER2-TK was first assessed. The results showed that V_HH17 significantly binding and inhibiting tyrosine kinase phosphorylation. Furthermore, R9V_HH17 could inhibit the native target expressed in HER2-positive cells and induce cell death. Cell growth was assayed using the alamarBlue™ cell viability assay in one normal and three cancer cell lines with variable HER2 expression: NIH/3 T3 (mouse fibroblast), MDA-MB-231 (triple-negative breast cancer), A431 (EGFR-positive epidermoid carcinoma) and BT-474 (HER2-positive human breast cancer).

Table II. The predictive residue interactions between V_HH17 with HER2-TK active-site along with the mode of interaction

Kinase domain of Her2		V_HH17		Interactive bond
Residue(s)	Domain	Residue(s)	Domain	
Ser728	Phosphate-binding loop	Arg113	CDR-3	Hydrogen bond
Ala730	Phosphate-binding loop	Leu110	CDR-3	Hydrophobic bond
Ala730	Phosphate-binding loop	Val112	CDR-3	Hydrophobic bond
Ala730	Phosphate-binding loop	Ala108	CDR-3	Hydrogen bond
Ala730	Phosphate-binding loop	Leu110	CDR-3	Hydrogen bond
Phe731	Phosphate-binding loop	Ile103	FR-3	Hydrophobic bond
Phe731	Phosphate-binding loop	Trp106	CDR-3	Hydrophobic bond
Phe731	Phosphate-binding loop	Ala108	CDR-3	Hydrophobic bond
Phe731	Phosphate-binding loop	Gly107	CDR-3	Hydrogen bond
Val734	Phosphate-binding loop	Ile109	CDR-3	Hydrophobic bond
Arg756	α-Helix C	Ser30	CDR-1	Hydrogen bond
Arg756	α-Helix C	Ser53	CDR-2	Hydrogen bond
Arg756	α-Helix C	Thr28	CDR-1	Hydrogen bond
Glu757	α-Helix C	Ser30	CDR-1	Hydrogen bond
Asn758	α-Helix C	Thr28	CDR-1	Hydrogen bond
Asn758	α-Helix C	Tyr29	CDR-1	Hydrogen bond
Asn758	α-Helix C	Ser30	CDR-1	Hydrogen bond
Ser760	α-Helix C	Ile103	CDR-3	Hydrogen bond
Ala763	α-Helix C	Trp106	CDR-3	Hydrophobic bond
Glu766	α-Helix C	Trp106	CDR-3	Hydrogen bond
Ile767	α-Helix C	Trp106	CDR-3	Hydrophobic bond
Ile767	α-Helix C	Ala108	CDR-3	Hydrophobic bond
Arg844	Catalytic loop	Trp106	CDR-3	Hydrogen bond
Arg844	Catalytic loop	Trp106	CDR-3	Cation–π interaction
Arg849	Catalytic loop	Ile109	CDR-3	Hydrogen bond
Gly865	Activation loop	Ala108	CDR-3	Hydrogen bond
Leu866	Activation loop	Ala108	CDR-3	Hydrophobic bond
Leu866	Activation loop	Ile109	CDR-3	Hydrophobic bond
Leu866	Activation loop	Leu110	CDR-3	Hydrophobic bond
Ala867	Activation loop	Trp106	CDR-3	Hydrophobic bond
Tyr877	Activation loop	Trp106	CDR-3	Hydrophobic bond
Tyr877	Activation loop	Trp106	CDR-3	Hydrogen bond
Asp880	Activation loop	Ser105	CDR-3	Hydrogen bond
Asp880	Activation loop	Trp106	CDR-3	Hydrogen bond
Lys883	Activation loop	GLy111	CDR-3	Hydrogen bond
Lys883	Activation loop	Tyr117	CDR-3	Hydrogen bond
Lys883	Activation loop	Tyr117	CDR-3	Cation–π interaction
Lys883	Activation loop	Tyr115	CDR-3	Cation–π interaction
Val884	Activation loop	Leu110	CDR-3	Hydrophobic bond
Pro885	Activation loop	Leu110	CDR-3	Hydrophobic bond

Following 72 h of continuous exposure to the nanobodies or lapatinib, all cell lines showed a dose-dependent inhibition of cell growth (Fig. 7). The estimated $R9V_HH17$ IC_{50} values were 1282 nM for MDA-MB-231, 314 nM for A431 and 41 nM for BT-474 cells. A comparison of the IC_{50} values among the cell lines revealed that $R9V_HH17$ had the lowest mean IC_{50} compared to the others in BT-474, whereas the other three cell lines were significantly less sensitive to $R9V_HH17$. In the A431 cancer cell lines, $R9V_HH17$ had an IC_{50} value 3-fold higher than that of lapatinib (314 versus 105 nM, respectively). Conversely, in NIH/3 T3 and MDA-MB-231 cells, low levels of inhibition were observed for all inhibitors. By contrast, R2 and V_HH17 had a slight influence on all the cell lines tested. Additionally, the $R9V_HH17$ also demonstrated the cell penetrability on SKBR3, breast cancer cell (Supplement Fig. 4). We concluded that inhibition of $R9V_HH17$ was specific for HER2-expressing BT-474 breast cancer cells. No effect was observed in control NIH/3 T3 cells.

$R9V_HH17$ preserve the binding property of V_HH17 to HER2-TK

We then performed a SPR assay to test the binding affinity of $R9V_HH17$ compared to V_HH17, R2, R9R2 and lapatinib for HER2-TK. The results revealed that $R9V_HH17$, V_HH17 and lapatinib had affinity for HER2-TK. As shown in Fig. 8 and Supplement Fig. 5, the binding affinity between nanobodies and HER2-TK or EGFR-TK were estimated in terms of the dissociation constant (KD), calculated using a Trace Drawer 1.9.1 software (Ridgeview Instruments). The K_D value between V_HH17 and HER2-TK was 7.49×10^{-7} M and that between $R9V_HH17$ and HER2-TK was 3.74×10^{-7} M (Table III). R2 nanobody and lapatinib used as negative and positive control, respectively (Fig. 8 and Table III). In addition, immunofluorescence binding assay demonstrate that the binding affinity of V_HH17 and $R9V_HH17$ were higher than that of R2 and R9R2 to HER2-TK (Supplement Fig. 3). The results showed that the use of cell-penetrable peptide tagging did not negate the binding affinity of the nanobodies to target

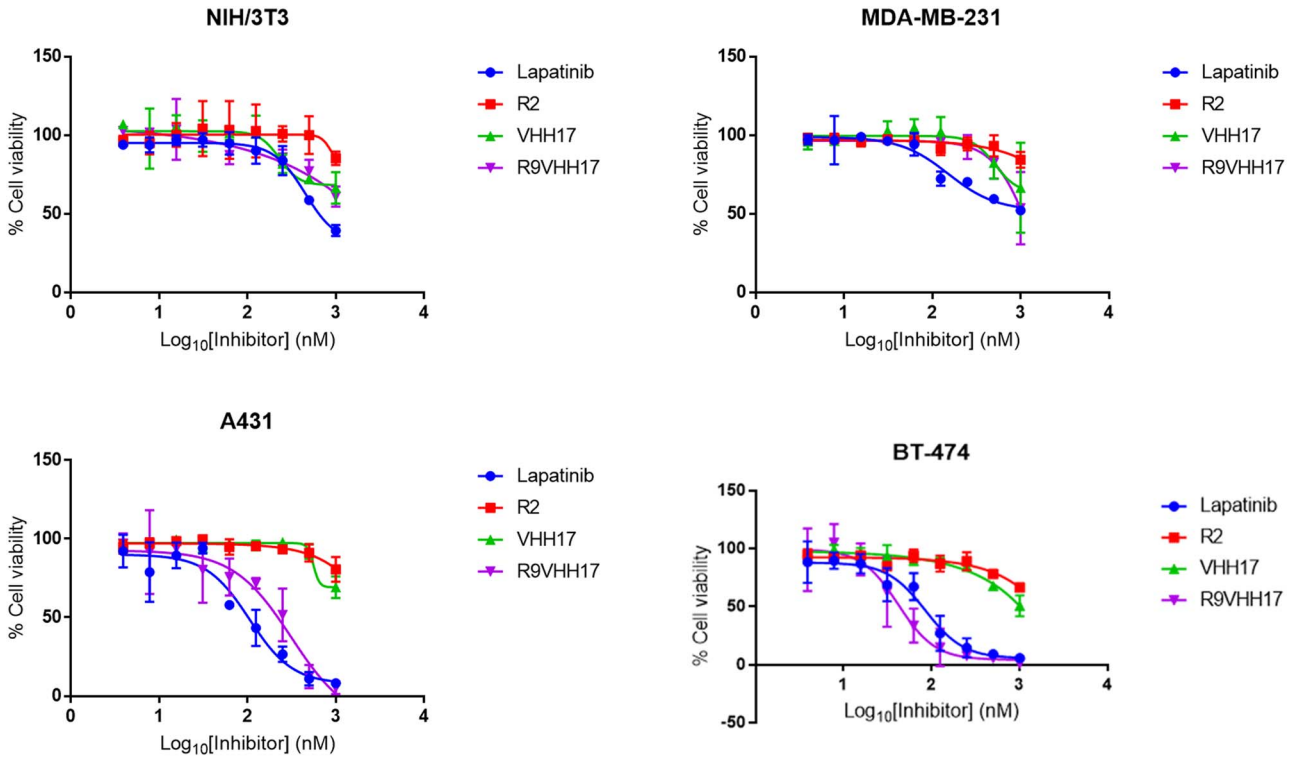

Fig. 7. Growth inhibitory effects of drug and nanobody treatments in the NIH/3 T3(mouse fibroblast(nontumor cells)), MDA-MB-231(triple-negative breast cancer), A431 (EGFR-positive epidermoid carcinoma) and BT-474 (HER2-positive human breast cancer). Cells were treated with lapatinib, R2 (irrelevant nanobody), VHH17, and R9VHH17 for 3 days, and alamarBlue™ reagent was added for the last 4 h. The results are expressed as mean ± SD of triplicate experiments.

proteins. Moreover, the binding affinity of V_HH17 to HER2-TK was higher than that of the EGFR-TK.

Discussion

The potential applications of camelid VHH single domains for diagnostic and therapeutic use have been reviewed (Leow *et al.,* 2018; Tillib 2020). Many nanobody-based biological agents showed anticancer activity in preclinical studies (Bannas *et al.,* 2017; Kijanka *et al.,* 2015). Especially HER2-targeted therapy is useful in the treatment of HER2-positive breast cancer. The nanobodies against the HER2-ECD have been used for antitumor therapeutic applications (Ding *et al.,* 2015; Gray *et al.,* 2016; Wu *et al.,* 2018) and nanobody-based molecular imaging and image-guided surgery (Vaneycken *et al.,* 2011; Kijanka *et al.,* 2013; Oliveira *et al.,* 2013; Pruszynski *et al.,* 2014; Keyaerts *et al.,* 2016; Khaleghi *et al.,* 2017; Altunay *et al.,* 2020). This study aimed to generate novel nanobodies as HER2-kinase domain inhibitors and evaluate their ability to block kinase phosphorylation activity, which reduces the rate of cancer cell proliferation and slows the progression of the disease. In this report, the humanized phage display library was used to screen HER2-TK-specific nanobodies, and initially, three single-domain antibody candidates were identified that more specifically bound to HER2-TK than to EGFR-TK, VH4, V_HH17 and VH22. Their potential HER2 kinase inhibitory activities were evaluated. Their IC_{50} values were similar to those for lapatinib, especially V_HH17 was more active than the other single-domain antibodies. Therefore, V_HH17 was further used to study whether its binding to HER2-TK was related to the A-loop. V_HH17 was mixed with lapatinib to observe the competitive binding effect on the ATP-binding site, and it was confirmed that lapatinib interfered with V_HH17 binding. This study indicated the possibility that the HER2-TK inhibitory effect of V_HH17 is caused by binding overlap to the ATP-binding site. Furthermore, mimotope mapping was used to identify the pocket where the V_HH17 docked onto HER2-TK. Interestingly, most of the mimotope sequence cloud was mapped near the A-loop of HER2-TK. Molecular docking revealed that V_HH17 was bound into the ATP-binding pocket of HER2-TK, which could lead to partial inhibition of kinase phosphorylation. Thus, V_HH17 must at least partly overlap with that of lapatinib. Additionally, the tagging of a cell-penetrable peptide to the N-terminal of V_HH17, resulting in $R9V_HH17$, enhanced nanobody penetration into the target cells and did not impede the functions of the nanobody. The cell viability assay showed that the estimated IC_{50} values of lapatinib and $R9V_HH17$ on BT-474 were 20- to 50-fold higher than that of the kinase-inhibition assay. Because in cell-based assay, the nanobody takes time to penetrate the cell before it reaches the target protein, moreover, the cancer cells themselves have another signaling pathway to regulate growth, thus making the IC_{50} higher than the enzymatic-inhibition assay. Additionally, medium content and final volume for cell culture, confluency of starting cell culture and initially inoculated cell number can affect the results. Regarding $R9V_H$ H17, the highest cell viability reduction was observed in BT-474 cells (Fig. 7). Taken together, these data indicate that the effect of $R9V_HH17$ is cell-specific and exerts dose-dependent cytotoxic effects in HER2-expressing breast cancer cells, with no effects being observed in normal cells.

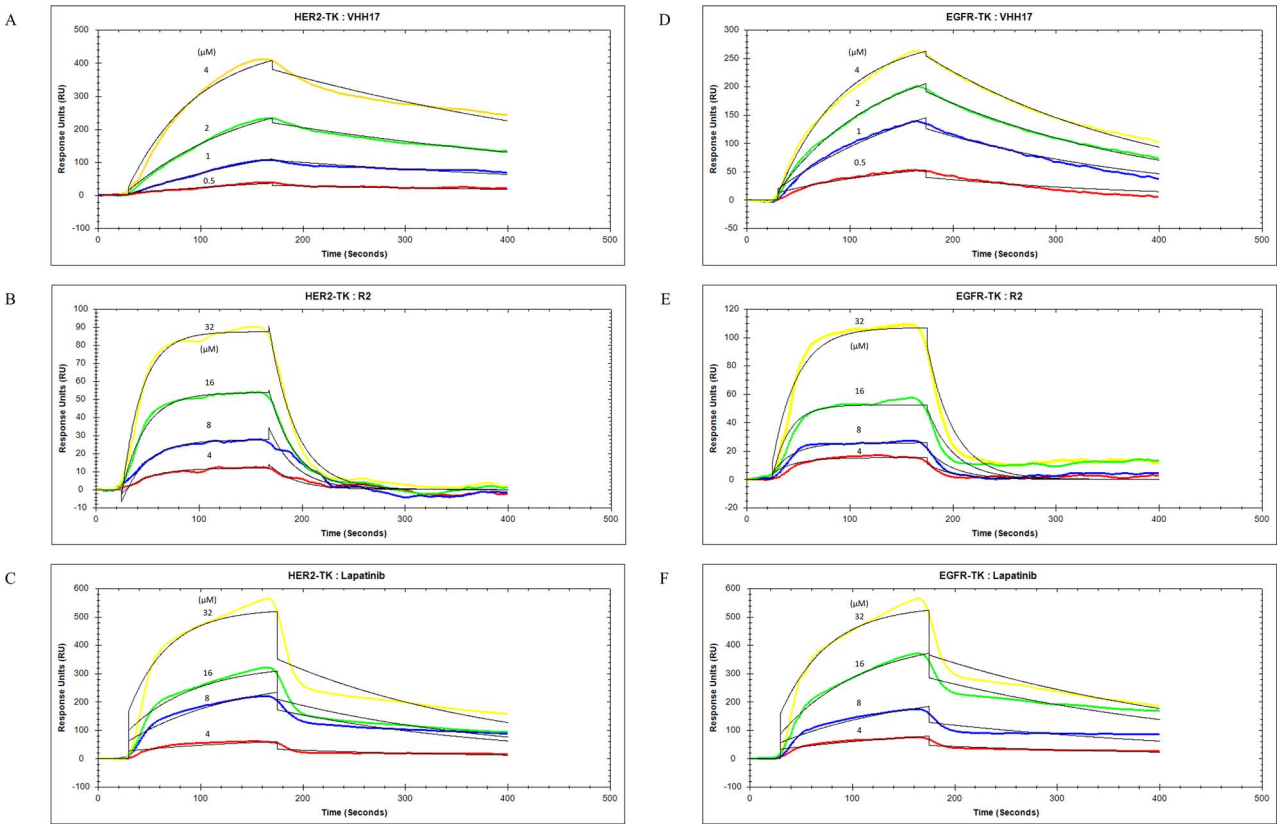

Fig. 8. Surface Plasmon Resonance (SPR) analysis of binding between VHH17 (A), R2 (B) or lapatinib (C) to HER2-TK and VHH17 (D), R2 (E) or lapatinib (F) to EGFR-TK protein. The two-dilutions of purified nanobodies and lapatinib (at the indicated concentrations) were flown at 30 μl/min in running buffer and sensorgrams were generated and analyzed with Trace Drawer 1.9.1 software (Ridgeview Instruments). Binding parameters are shown in Table III.

Table III. Binding parameters of lapatinib, R2, R9R2, V_HH17 and R9-V_HH17 binding to immobilized HER2-TK and EGFR-TK are determined by SPR measurements and analyzed with TraceDrawer 1.9.1 software (Ridgeview Instruments)

Ligand	Analytes	k_a (1/(M×s))	est. error	k_d (1/s)	est. error	K_D (M)	est. error
HER2-TK	Lapatinib	7.39E+02	±7.17e2	4.18E−03	±8.26e−6	5.66E−06	±9.44e−5
	R2	4.10E+02	±4.28e1	3.85E−02	±4.75e−7	9.39E−05	±9.89e−6
	R9R2	2.40E+02	±2.53e2	5.13E−02	±2.01e−6	2.14E−04	± − 2.02e−3
	V_HH17	3.05E+03	±2.72e1	2.29E−03	±1.03e−6	7.49E−07	±7.00e−9
	R9V_HH17	6.80E+03	±1.20e3	2.54E−03	±1.70e−5	3.74E−07	±7.09e−8
EGFR-TK	Lapatinib	5.66E+02	±2.41e2	3.24E−03	±5.32e−6	5.72E−06	±2.99e−6
	R2	1.43E+03	±4.34e2	3.85E−02	±3.08e−6	2.70E−05	±9.05e−6
	V_HH17	2.85E+03	±2.23e1	4.44E−03	±4.04e−7	1.56E−06	±1.23e−8

The curve was fitted by nonlinear least squares regression using the 1:1 Langmuir binding model (theoretical sensorgrams in black). The errors represent the standard deviations based on at least three independent experiments.

Despite only one-round of bio-panning, the isolated nanobody exhibits the binding specificity, affinity and kinase-inhibition activity against HER2-TK. Further structural analysis of proteins may confirm these interactions between HER2-TK and V_H H17. Moreover, the R9V_H H17 carried cell-penetrability and growth-inhibition activity on HER2-expressing cancer cells. However, the nanobody can be engineered with other technologies to enhance its specific binding potential. In case of further *in vivo* studies, the development of drug transporter and tracking systems are necessary. Our work demonstrates the potential of a humanized-nanobody generated from the phage display library that is involved in the binding related to the ATP-binding pocket of HER2 that could inhibit HER2-TK phosphorylation and, finally, reduce breast cancer cell viability, making it a promising alternative HER2-kinase inhibitor.

Supplementary data

Supplementary data are available at *PEDS* online.

Acknowledgments

The authors thank the members of the Assoc. Prof. Dr Kiattawee's laboratory for suggestions and support on molecular cloning and protein preparation, Assoc. Prof. Dr Paul(P.M.P.) van Bergen en Henegouwen and Assoc. Prof. Dr Sabrina Oliveira's laboratory, Division of Cell Biology, Department of Biology, Faculty of Science, Utrecht University, the Netherlands, supported some parts of the nanobodies and cell-based assays work.

Funding

This study was funded by the Royal Golden Jubilee PhD Program (Grant no. PHD/0152/2557), National Research council of Thailand

(NRCT5-RSA63002–07), the Kasetsart University Research and Development Institute (KURDI (FF(KU)6.64), Bangkok, Thailand, and the Center for Advanced Studies in Nanotechnology for Chemical, Food and Agricultural Industries, Kasetsart University Institute for Advanced Studies.

Conflict of Interest

The authors declare that they have no conflicts of interest with the contents of this article.

References

Altunay, B., Morgenroth, A., Beheshti, M., Vogg, A., Wong, N.C.L., Ting, H.H., Biersack, H.J., Stickeler, E. and Mottaghy, F.M. (2020) *Eur. J. Nucl. Med. Mol. Imaging*, **48**, 1371–1389.

Arteaga, C.L., Sliwkowski, M.X., Osborne, C.K., Perez, E.A., Puglisi, F. and Gianni, L. (2012) *Nat. Rev. Clin. Oncol.*, **9**, 16–32.

Bachelot, T., Ciruelos, E., Schneeweiss, A. *et al.* (2019) *Ann. Oncol.*, **30**, 766–773.

Baker, J.H.E., Lindquist, K.E., Huxham, L.A., Kyle, A.H., Sy, J.T. and Minchinton, A.I. (2008) *Clin. Cancer Res.*, **14**, 2171–2179.

Bannas, P., Hambach, J. and Koch-Nolte, F. (2017) *Front. Immunol.*, **8**, 1–13.

Blackwell, K.L., Burstein, H.J., Storniolo, A.M. *et al.* (2010) *J. Clin. Oncol.*, **28**, 1124–1130.

Bose, R. (2013) *Clin. Cancer Res.*, **19**, 3331–3333.

Bose, R., Kavuri, S.M., Searleman, A.C. *et al.* (2013) *Cancer Discov.*, **3**, 224–237.

Brenke, R., Hall, D.R., Chuang, G.Y., Comeau, S.R., Bohnuud, T., Beglov, D., Schueler-Furman, O., Vajda, S. and Kozakov, D. (2012) *Bioinformatics*, **28**, 2608–2614.

Capelan, M., Pugliano, L., De Azambuja, E., Bozovic, I., Saini, K.S., Sotiriou, C., Loi, S. and Piccart-Gebhart, M.J. (2013) *Ann. Oncol.*, **24**, 273–282.

D'Amato, V., Raimondo, L., Formisano, L., Giuliano, M., de Placido, S., Rosa, R. and Bianco, R. (2015) *Cancer Treat. Rev.*, **41**, 877–883.

Dawood, S., Gonzalez-Angulo, A.M., Peintinger, F., Broglio, K., Symmans, W.F., Kau, S.W., Islam, R., Hortobagyi, G.N. and Buzdar, A.U. (2007) *Cancer*, **110**, 1195–1200.

D'Huyvetter, M., de Vos, J., Xavier, C. *et al.* (2017) *Clin. Cancer Res.*, **23**, 6616–6628.

Ding, L., Tian, C., Feng, S., Fida, G., Zhang, C., Ma, Y., Ai, G., Achilefu, S. and Gu, Y. (2015) *Theranostics*, **5**, 378–398.

Ferretti, G., Papaldo, P., Fabi, A., Carlini, P., Felici, A. and Cognetti, F. (2006) *Oncologist*, **11**, 853–854.

Gray, M.A., Tao, R.N., Deporter, S.M., Spiegel, D.A. and McNaughton, B.R. (2016) *Chem. Bio. Chem.*, **17**, 155–158.

Hoogenboom, H.R., De Brune, A.P., Hufton, S.E., Hoet, R.M., Arends, J.W. and Roovers, R.C. (1998) *Immunotechnology*, **4**, 1–20.

Hudelist, G., Köstler, W.J., Attems, J. *et al.* (2003) *Br. J. Cancer*, **89**, 983–991.

Joensuu, H., Kellokumpu-Lehtinen, P.L., Bono, P. *et al.* (2006) *N. Engl. J. Med.*, **354**, 809–820.

Källberg, M., Margaryan, G., Wang, S., Ma, J. and Xu, J. (2014) **1137**, 1–15.

Keyaerts, M., Xavier, C., Heemskerk, J. *et al.* (2016) *J. Nucl. Med.*, **57**, 27–33.

Khaleghi, S., Rahbarizadeh, F., Ahmadvand, D. and Hosseini, H.R.M. (2017) *Cell. Mol. Bioeng.*, **10**, 263–272.

Kijanka, M., Dorresteijn, B., Oliveira, S. and van Bergen en Henegouwen, P.M.P. (2015) *Nanomedicine*, **10**, 161–174.

Kijanka, M., Warnders, F.J., el Khattabi, M., Lub-De Hooge, M., van Dam, G.M., Ntziachristos, V., de Vries, L., Oliveira, S. and van Bergen en Henegouwen, P.M.P. (2013) *Eur. J. Nucl. Med. Mol. Imaging*, **40**, 1718–1729.

Kulkeaw, K., Sakolvaree, Y., Srimanote, P. *et al.* (2009) *J. Proteomics*, **72**, 270–282.

Leow, C.H., Cheng, Q., Fischer, K. and McCarthy, J. (2018) *Antibody Eng.*, 175–204.

Marty, M., Cognetti, F., Maraninchi, D. *et al.* (2005) *J. Clin. Oncol.*, **23**, 4265–4274.

Von Minckwitz, G., Procter, M., De Azambuja, E. *et al.* (2017) *N. Engl. J. Med.*, **377**, 122–131.

O'Donovan, N., Byrne, A.T., O'Connor, A.E., McGee, S., Gallagher, W.M. and Crown, J. (2011) *Invest. New Drugs*, **29**, 752–759.

Oliveira, S., Heukers, R., Sornkom, J., Kok, R.J. and van Bergen en Henegouwen, P.M.P. (2013) *J. Control. Release*, **172**, 607–617.

Pruszynski, M., D'Huyvetter, M., Bruchertseifer, F., Morgenstern, A. and Lahoutte, T. (2018) *Mol. Pharm.*, **15**, 1457–1466.

Pruszynski, M., Koumarianou, E., Vaidyanathan, G., Revets, H., Devoogdt, N., Lahoutte, T., Lyerly, H.K. and Zalutsky, M.R. (2014) *J. Nucl. Med.*, **55**, 650–656.

Laskowski, R.A. and Swindells, M.B. (2011) *J. Chem. Inf. Model.*, **51**, 2778–2786.

Reiter, Y., Schuck, P., Boyd, L.F. and Plaksin, D. (1999) *J. Mol. Biol.*, **290**, 685–698.

Revets, H., De Baetselier, P. and Muyldermans, S. (2005) *Expert Opin. Biol. Ther.*, **5**, 111–124.

Roskoski, R. (2004) *Biochem. Biophys. Res. Commun.*, **319**, 1–11.

Ross, J.S., Slodkowska, E.A., Symmans, W.F., Pusztai, L., Ravdin, P.M. and Hortobagyi, G.N. (2009) *Oncologist*, **14**, 320–368.

Ross, J.S., Wang, K., Sheehan, C.E. *et al.* (2013) *Clin. Cancer Res.*, **19**, 2668–2676.

Rudnick, S.I. and Adams, G.P. (2009) *Cancer Biother. Radiopharm.*, **24**, 155–161.

Sarma, V.R., Silverton, E.W., Davies, D.R. and Terry, W.D. (1971) *J. Biol. Chem.*, **246**, 3753–3759.

Seetaha, S., Ratanabanyong, S. and Choowongkomon, K. (2019) *Appl. Microbiol. Biotechnol.*, **103**, 8427–8438.

Sheikholeslami, F., Rasaee, M.J., Shokrgozar, M.A., Dizaji, M.M., Rahbarizadeh, F. and Ahmadvande, D. (2010) *Lab. Med.*, **41**, 69–76.

Siontorou, C.G. (2013) *Int. J. Nanomedicine*, **8**, 4215–4227.

Slamon, D.J., Clark, G.M., Wong, S.G., Levin, W.J., Ullrich, A. and McGuire, W.L. (1987) *Science*, **235**, 177–182.

Smith, K.L., Dang, C. and Seidman, A.D. (2006) *Expert Opin. Drug Saf.*, **5**, 619–629.

Speyer, J. (2002) *J. Clin. Oncol.*, **20**, 1156–1157.

Stamos, J., Sliwkowski, M.X. and Eigenbrot, C. (2002) *J. Biol. Chem.*, **277**, 46265–46272.

Thanongsaksrikul, J., Srimanote, P., Maneewatch, S., Choowongkomon, K., Tapchaisri, P., Makino, S.I., Kurazono, H. and Chaicumpa, W. (2010) *J. Biol. Chem.*, **285**, 9657–9666.

Tillib, S.V. (2020) *Mol. Biol.*, **54**, 317–326.

Turke, A.B., Song, Y., Costa, C., Cook, R., Arteaga, C.L., Asara, J.M. and Engelman, J.A. (2012) *Cancer Res.*, **72**, 3228–3237.

Vaneycken, I., Devoogdt, N., van Gassen, N., Vincke, C., Xavier, C., Wernery, U., Muyldermans, S., Lahoutte, T. and Caveliers, V. (2011) *FASEB J.*, **25**, 2433–2446.

Wu, X., Chen, S., Lin, L., Liu, J., Wang, Y., Li, Y., Li, Q. and Wang, Z. (2018) *Transl. Oncol.*, **11**, 366–373.

Xavier, C., Blykers, A., Vaneycken, I., D'Huyvetter, M., Heemskerk, J., Lahoutte, T., Devoogdt, N. and Caveliers, V. (2016) *Nucl. Med. Biol.*, **43**, 247–252.

Xu, D. and Zhang, Y. (2011) *Biophys. J.*, **101**, 2525–2534.

Yarden, Y. and Sliwkowski, M.X. (2001) *Nat. Rev. Mol. Cell Biol.*, **2**, 127–137.

Yu, D. and Hung, M.C. (2000) *Oncogene*, **19**, 6115–6121.